Virologica Sinica 38 (2023) 373–379

Contents lists available at ScienceDirect

Virologica Sinica

journal homepage: www.keaipublishing.com/en/journals/virologica-sinica
www.virosin.org

Research Article

Construction and characterization of a synthesized herpes simplex virus H129-Syn-G2

Han Xiao [a,b], Hengrui Hu [a], Yijia Guo [a,b], Jiang Li [a], Le Wen [a], Wen-Bo Zeng [a,*], Manli Wang [a,b,*], Min-Hua Luo [a,b,*], Zhihong Hu [a,*]

[a] State Key Laboratory of Virology, Center for Biosafety Mega-Science, Wuhan Institute of Virology, Chinese Academy of Sciences, Wuhan, 430071, China
[b] University of Chinese Academy of Sciences, Beijing, 100049, China

ARTICLE INFO

Keywords:
Herpes simplex virus type 1 (HSV-1)
Neuronal circuit tracers
H129-Syn-G2
H129-G4
Synthetic biology

ABSTRACT

Herpes simplex virus type 1 (HSV-1) causes lifelong infections worldwide, and currently there is no efficient cure or vaccine. HSV-1-derived tools, such as neuronal circuit tracers and oncolytic viruses, have been used extensively; however, further genetic engineering of HSV-1 is hindered by its complex genome structure. In the present study, we designed and constructed a synthetic platform for HSV-1 based on H129-G4. The complete genome was constructed from 10 fragments through 3 rounds of synthesis using transformation-associated recombination (TAR) in yeast, and was named H129-Syn-G2. The H129-Syn-G2 genome contained two copies of the *gfp* gene and was transfected into cells to rescue the virus. According to growth curve assay and electron microscopy results, the synthetic viruses exhibited more optimized growth properties and similar morphogenesis compared to the parental virus. This synthetic platform will facilitate further manipulation of the HSV-1 genome for the development of neuronal circuit tracers, oncolytic viruses, and vaccines.

1. Introduction

Herpes simplex virus type 1 (HSV-1) is a prevalent pathogen with severe clinical manifestation, such as cold sores, herpes genitalis, keratitis, and encephalitis (Bradshaw and Venkatesan, 2016; Ludlow et al., 2016). HSV-1 establishes latency in ganglia after lytic infection, and exhibits periodic reactivation and recurrent infection, causing a worldwide epidemic (Whitley and Roizman, 2001). HSV-1 has been extensively studied for decades and HSV-1-derived tools have been applied in several fields. The study of HSV-1-based neuronal circuit tracers are beneficial in neuroscience (Nassi et al., 2015; Xu et al., 2020; Yang et al., 2020). Oncolytic HSV (oHSV) is one of the most promising candidates for oncolytic therapy (Abd-Aziz and Poh, 2021; Aldrak et al., 2021). Despite extensive applications of HSV-1 in life science and biomedicine, the complexity of the HSV-1 genome manipulation hinders further investigation and application of HSV-1 (Szpara et al., 2010; Dogrammatzis et al., 2020).

HSV-1 has a large linear dsDNA genome of about 152 kb, with a high G/C content of approximately 68%. The HSV-1 genome consists of two unique regions: unique long (UL) and unique short (US), which are flanked by inverted repeat regions (TR_L, IR_L, IR_S and TR_S). It encodes at least 84 different open reading frames (ORFs) (Roizman, 1996). Although most ORFs are distributed in the UL and US, some ORFs are located in inverted repeat regions that have higher G/C content and contain variable-number tandem repeats (Kuny and Szpara, 2022). Because of the high G/C content and repeat sequences, cloning certain regions in the HSV-1 genome is extremely difficult (Goldin et al., 1981; Perng et al., 1994). Previous approaches to modification of HSV-1 genome mainly rely on homologous recombination in cells (Chou et al., 1990; Mineta et al., 1995) or bacterial artificial chromosome (BAC) technology (Messerle et al., 1997), however, the structural complexity and high G/C content of HSV-1 genome limit the efficiency of genomic engineering of HSV-1.

The development of synthetic biology provides novel approaches for genome engineering of HSV-1. The first *de novo* synthesis of the KOS strain of HSV-1 (HSV-1 KOS), was published in 2017 (Oldfield et al., 2017). As a model strain, the HSV-1 KOS is less virulent than other HSV-1 strains (Perng et al., 2002). The synthesized HSV-1 KOS showed growth properties similar to those of the wild-type HSV-1 KOS. The establishment of synthetic platform could facilitate the virological studies involving systematic analysis of multiple viral genes and complex sequences in viral genome (Vashee et al., 2017; Grzesik et al., 2018; Hu et al., 2021).

* Corresponding authors.
E-mail addresses: zengwb@wh.iov.cn (W.-B. Zeng), wangml@wh.iov.cn (M. Wang), luomh@wh.iov.cn (M.-H. Luo), huzh@wh.iov.cn (Z. Hu).

https://doi.org/10.1016/j.virs.2023.03.005
Received 27 December 2022; Accepted 15 March 2023
Available online 20 March 2023

To date, many different HSV-1 strains have been reported and showed different phenotypes (Szpara et al., 2014). The first genome sequence of HSV-1 (HSV-1 strain 17) was published in 1988 (McGeoch et al., 1988), and afterward, genome sequencing of other strains, including F, H129, Mckrae and KOS were reported (Szpara et al., 2010; Macdonald et al., 2012a, 2012b). Sequencing results of different strains revealed single nucleotide polymorphisms, insertions, and deletions, which may contribute to different phenotypes, such as virulence and spreading characteristics of the different strains. Strain H129 was clinically isolated from a patient with herpes encephalitis (Dix et al., 1983). The spreading characteristics of H129 differs from other HSV-1 strains, showing an anterograde transneuronal phenotype in the central nervous system (Sun et al., 1996). Genome sequencing highlighted unique amino acid changes of H129 which were mainly located in UL1 (gL), UL36, RL1 (ICP34.5), RL2 (ICP0) and US7 (gI). Some of these proteins are involved in virus attachment and neurovirulence, suggesting that these changes may contribute to the unique anterograde spread phenotype of H129 (Szpara et al., 2010). Owing to its unique spread phenotype, H129 has been widely applied in neuronal circuit tracing (Su et al., 2019, 2020; Yang et al., 2022). H129-G4, for example, is an H129 derived anterograde neuronal circuit tracer that contains four copies of *gfp* genes in the genome (Fig. 1A) (Zeng et al., 2017). The results of *in vivo* tracing in mouse brains showed that H129-G4 is capable of visualizing the morphological details of neurons and projection pathways of correlated neurons (Li et al., 2017; Yu et al., 2017).

In this study, we focused on developing a synthesized HSV-1 derived from H129-G4. The genome was designed and built from 10 fragments using transformation-associated recombination (TAR) (Kouprina and Larionov, 2008) in yeast. The synthetic genome was transfected into Vero cell to rescue the virus, and the properties of the synthesized virus were compared with those of the parental H129-G4.

2. Materials and methods

2.1. Cell culture, virus, strains and plasmid

Vero cells (ATCC#CCL-81) were purchased from ATCC and cultured at 37 °C with 5% CO_2 in Dulbecco's modified Eagle's medium with 10% fetal bovine serum (Gibco, USA). The H129-G4 virus was amplified in Vero cells, and the viral titer was measured using plaque assay (Zeng et al., 2017). *E. coli* strain EPI300, *S. cerevisiae* strain VL6-48, and TAR cloning vector pGF were initially provided by Prof. G.F. Xiao from the Wuhan Institute of Virology, Chinese Academy of Sciences, and maintained in our laboratory (Shang et al., 2017).

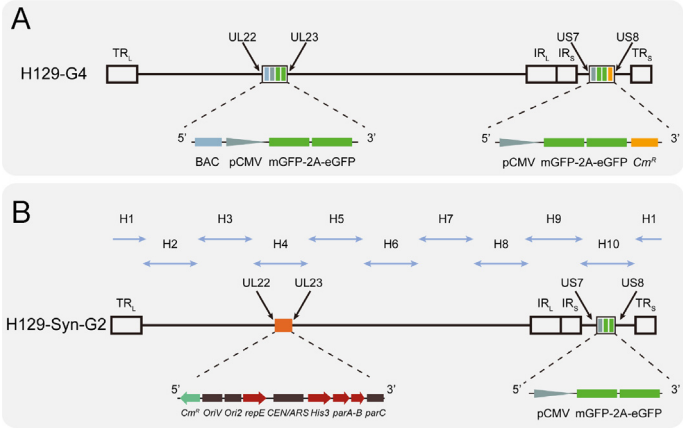

Fig. 1. Schematic diagram of H129-G4 and H129-Syn-G2 genomes. **A** Schematic of the genome of parental virus H129-G4. It contains a copy of mGFP-2A-eGFP cassette driving by CMV promoter (pCMV) inserted between *UL22* and *UL23*, and another copy of GFP cassette and a chloramphenicol resistance gene (Cm^R) between *US7* and *US8*. **B** Schematic of the synthetic genome H129-Syn-G2. H1–H10 fragments were distributed on the top of the genome; the location and details of the pGF vector and the GFP cassette were shown under the genome.

2.2. Synthesis of H129-Syn-G2 genome

The H129-Syn-G2 genome was designed from 10 fragments (H1–H10) using the H129-G4 genome as the template (Fig. 1A). The synthesis of the H129-Syn-G2 genomic DNA was performed in three steps, as shown in Fig. 2. In the first step, H4 and H10 DNA fragments were amplified by PCR using H129-G4 DNA as the template; the primers are presented in Supplementary Table S1. Other H-level fragments were generated from sheared H129-G4 DNA using protocols similar to those reported by (Oldfield et al., 2017). Vectors for synthesis were amplified by PCR using 2× Phanta Master Mix (Vazyme, China) with pGF as the template, and the primers are presented in Supplementary Table S1. The DNA of each H fragment and the respective PCR-amplified vector were co-transformed into spheroplasts of *S. cerevisiae* VL6-48, and TAR cloning was performed according to a previously published protocol (Kouprina and Larionov, 2008). The positive cloned plasmids from yeast were then electroporated into *E. coli* EPI300 competent cells for maintenance and large-scale amplification. In step 2, individual H fragments were digested from pGF-H plasmids with *Pme*I, and three H fragments (H1, H2 and H3; H5, H6 and H7; and H8, H9 and H10) were grouped together and cotransformed with the PCR-amplified vector fragments into yeast to synthesize the intermediate fragment. Finally, the three intermediate fragments digested by *Pme*I and *Pme*I-linearized pGF-H4 were transformed into yeast spheroplasts for TAR cloning of the complete genome (step 3 in Fig. 2). At each step, positive clones were confirmed by PCR and restriction enzyme assays. For the intermediate fragments and the complete genome, the correct assembly of the junctions was also detected by PCRs using the primers listed in Supplementary Table S2. Electrophoresis was simulated using SnapGene (version 4.2.4) (Shang et al., 2017).

2.3. Genome sequencing of H129-Syn-G2

The DNA of H129-Syn-G2 was extracted from *E. coli* using the Plasmid Mini Kit (QIAGEN, Germany) and processed for Illumina sequencing following the standard protocol at the Sequencing Platform of Huazhong Agricultural University (Wuhan, China). Quality control of raw data was examined using FastQC (version 0.11.9), the reads were assembled using Bowtie2 (version 2.3.5.1) with default settings, and the assembled sequences were analyzed using Tablet (version 1.21.02.08).

2.4. Transfection and infection assays of H129-Syn-G2

Purified H129-Syn-G2 (2.5 μg) was transfected into African green monkey kidney Vero cells (8×10^5 in 6-wells plates) using Lipofectamine 3000 reagent (Thermo Fisher, USA). H129-G4 was also transfected as a positive control. Culture supernatants were harvested at 96 h post-transfection (p.t.) and stored at −80 °C. For the infection assay, 50 μL supernatant was inoculated into 2×10^6 Vero cells, and the culture supernatant was harvested at 48 h post infection (p.i.) and stored at −80 °C. The fluorescence of both samples was observed at 48 h and 96 h p.t. for the transfection assay and at 24 h and 72 h p.i. for the infection assay. The viral titer was detected by plaque assay as previously described (Zeng et al., 2017). The plaques with fluorescence were captured by fluorescent microscopy and plaque size was measured using imageJ (version 1.53t). Statistical difference between the plaque size of H129-G4 and H129-Syn-G2 were analyzed by Student *t* -test.

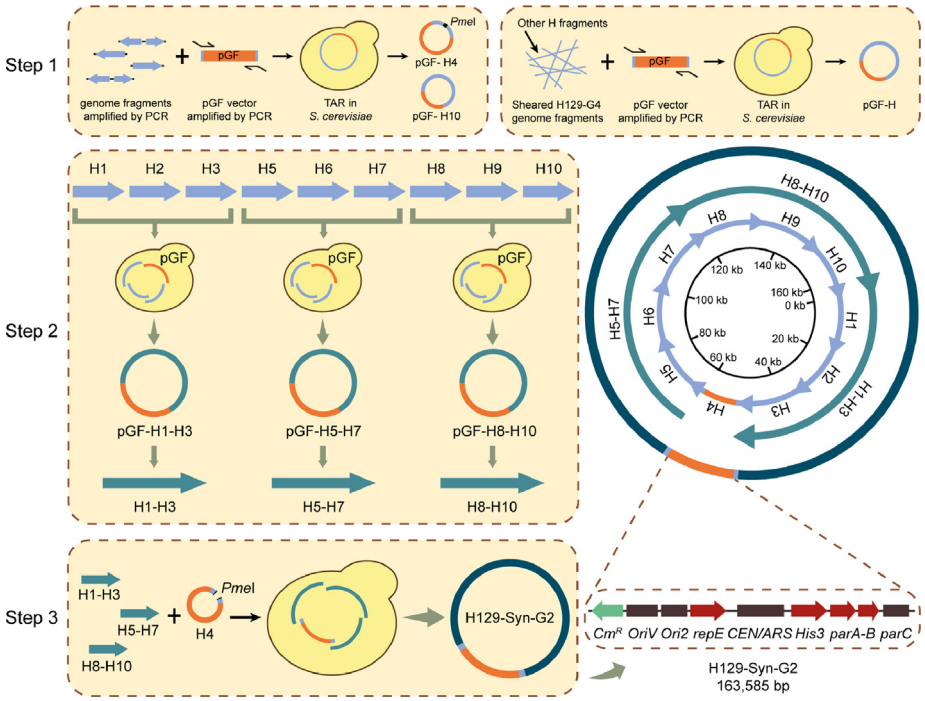

Fig. 2. Schematic flowchart of the synthesis of H129-Syn-G2. The synthetic genome was generated in three steps. First, H4 and H10 fragments were constructed from PCR-amplified genome fragments and pGF vector DNA, and other H fragments were constructed from the sheared genome of H129-G4 and PCR-amplified pGF vector DNA. The DNA fragments were cotransformed into yeast for transformation-associated recombination (TAR) cloning to generate pGF-H plasmids. Second, all H fragments, except H4, were recombined in sets of three to synthesize three intermediates: H1–H3, H5–H7, and H8–H10. Finally, three intermediate fragments and linearized pGF-H4 were cotransformed into yeast, and the complete genome was synthesized. The circular map of H129-Syn-G2 in the right panel presents the relative location of each level of genomic fragment among the genome and detailed information of the pGF vector cassette.

2.5. Growth curve assay

Vero cells (8×10^5 in 6-wells plates) were infected with H129-G4 and H129-Syn-G2 at multiplicity of infection (MOI) of 3 or 0.001 (PFU/cell). The supernatants of the infection were harvested at different time points, and the viral titer was detected using a plaque assay. Three independent biological repeats were performed and growth curves were plotted using GraphPad Prism 8.3.0 (GraphPad Software Inc., San Diego, CA, USA). Statistical differences between the growth curves of H129-G4 and H129-Syn-G2 were analyzed using a two-way ANOVA.

2.6. Transmission electron microscopy

Vero cells (1.2×10^6) were cultured in 60-mm dishes and separately infected with H129-G4 or H129-Syn-G2 at an MOI of 1. Infected cells were harvested at 12 and 18 h p.i. and processed for transmission electron microscopy using a method reported by Shang et al. (2017). The samples were observed and photographed using an FEI Tecnai G^2 20 TWIN (FEI, Carlsbad, California, USA) electron microscope at an accelerating voltage of 200 kV.

3. Result

3.1. Synthesis of H129-Syn-G2 genome

The synthetic HSV-1 genome was designed based on the H129-G4 genome, which contains a BAC cassette, four *gfp* genes (including mGFP and eGFP), and a chloramphenicol resistance (Cm^R) gene (Fig. 1A) (Zeng et al., 2017). The synthetic genome was designed to be synthesized from 10 overlapping genomic fragments (H1–H10), which were approximately 17 kb on average (Fig. 1B). Among these 10 fragments, H1 encompasses TR_L and TR_S, H2 to H8 cover the UL region, H9 contains IR_L and IR_S, and H10 covers the US region. Details of each genomic fragment are presented in Supplementary Table S3. Compared to the parental H129-G4 genome, two modifications were made to the synthetic genome (Fig. 1B). First, the BAC and mGFP-2A-eGFP cassette between *UL22* and *UL23* was replaced with the pGF vector sequence (Hou et al., 2016). Second, the Cm^R located between *US7* and *US8* in H10 was removed during synthesis of the H10 fragment. The synthetic genome, containing two *gfp* genes (mGFP and eGFP), was named H129-Syn-G2.

The H129-Syn-G2 genome was synthesized following the three-step strategy shown in Fig. 2. First, 10 H fragments were individually cloned into the pGF vector using TAR cloning. Technically, H4 and H10 sequences were generated by PCR amplification as designed, whereas the other fragments were obtained by shearing H129-G4 BAC DNA. These fragments (H1–H10) were cloned individually into the pGF vector *via* TAR in yeast. Second, the H fragments (except H4) were combined into three groups to synthesize intermediate fragments (H1–H3, H5–H7 and H8–H10) *via* TAR in yeast. Finally, linearized intermediate fragments and H4 were co-transformed into yeasts to synthesize the complete genome.

During synthesis, quality control using PCR and restriction enzyme digestion were performed at each step of cloning. Supplementary Fig. S1 shows the restriction enzyme profiles of plasmid DNAs containing individual H fragments (Supplementary Fig. S1A) or intermediate fragments (Supplementary Fig. S1B). The results of restriction enzyme analysis of the complete genome were shown in Fig. 3. Physical maps of H129-G4 (G4) and H129-Syn-G2 (Syn) digested with *Eco*RV, *Kpn*I, and *Hind*III are shown in Fig. 3A, and the predicted electrophoresis profiles are shown in Fig. 3B. The experimental results demonstrated that the H129-Syn-G2 displayed correct electrophoresis profiles, as expected (Fig. 3C).

High-throughput sequencing of H129-Syn-G2 was performed, and the results showed that there were three nucleotide (nt) point mutations compared to the sequence of H129-G4 (Table 1). The C-T mutation at

57,713 nt resulted in amino acid (aa) substitutions of UL23 (R20H) and UL24 (A3V), whereas the T-C mutation at 157,391 nt resulted in the I72V mutation of US11. The G-A mutation at 147,391 nt resulted in a synonymous aa mutation in the US6. No additional changes were observed except for those in the design.

3.2. Rescued H129-Syn-G2 exhibited more optimized growth properties than the parental virus

To rescue the synthetic virus, purified DNAs of H129-Syn-G2 and H129-G4 were transfected into Vero cells for the experiment and positive control, respectively. At 48 h p.t., green fluorescence was observed in both cultures, and the fluorescence signal increased significantly at 96 h p.t. The supernatants were harvested to infect Vero cells and the results showed that H129-Syn-G2 could establish a successful infection similar to that of H129-G4 (Fig. 4A).

Plaque assays were performed to investigate the cytopathogenic effects of these viruses. Both H129-G4 and H129-Syn-G2 produced visible plaques on the cell monolayers, but the plaque size of H129-G4 appeared to be smaller than that of H129-Syn-G2 (Fig. 4B). Because both viruses contain *gfp* genes in their genomes, we examined the plaques under fluorescent microscopy. The results confirmed that both viruses induced visible cytopathic effects and fluorescence-forming units, but the plaque size of H129-Syn-G2 was slightly larger than that of H129-G4 (Fig. 4C). For further comparison, 30 plaques were randomly selected from each virus, and the plaque sizes were measured. Statistical analysis confirmed that the plaque size of H129-Syn-G2 were significantly larger than that of H129-G4 ($P < 0.0001$) (Fig. 4D).

Table 1
The results of the genome sequencing of H129-Syn-G2[a].

Location	nt mutation[b]	Amino acid mutation[b]
64,492	C→T	R20H in UL23; A3V in UL24
154,714	G→A	Synonymous in US6
163,441	T→C	Synonymous in US10; I72V in US11

[a] The genome sequence of H129-Syn-G2 has been deposited in GenBank with accession no OQ077661.
[b] Mutation refers to the change from H129-G4 to H129-Syn-G2.

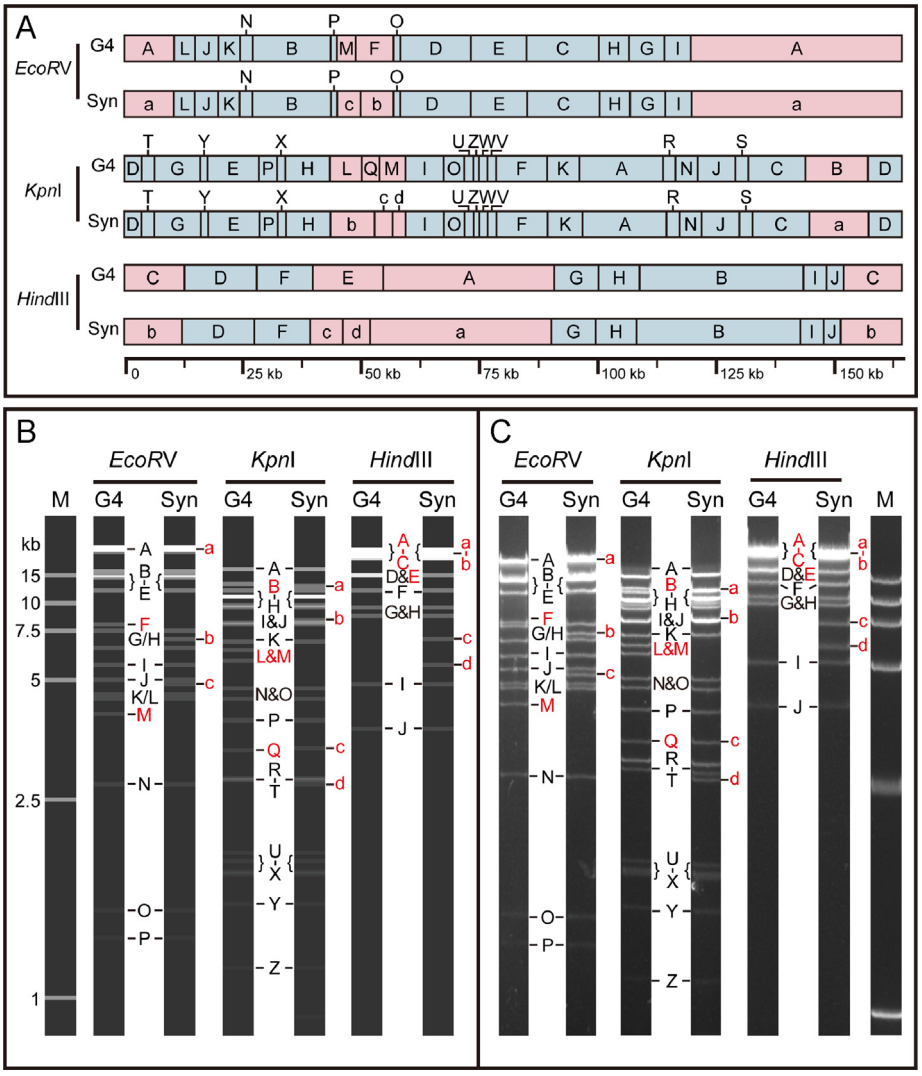

Fig. 3. Restriction enzyme analysis of the synthetic and parental genomes. **A** Physical maps of H129-G4 and H129-Syn-G2 genomes with *Eco*RV, *Kpn*I, and *Hind*III digestion. Digested genomic fragments were named alphabetically according to their length, from long to short. Fragments that were shared by both genomes are shown in light blue, while the differential fragments are marked in pink. **B** Computational prediction of restriction enzyme profiles of H129-G4 and H129-Syn-G2. **C** The experimental results of the restriction enzyme profiles of H129-G4 and H129-Syn-G2. In (**B**) and (**C**), the different fragments were indicated in red, G4, H129-G4; Syn, H129-Syn-G2.

To compare the replication dynamics of H129-Syn-G2 and parental virus, growth curve assay was conducted at MOI of 3 and MOI of 0.001, respectively, and the results are shown in Fig. 4E. For the MOI of 3 groups, the viral titers of H129-Syn-G2 were consistently higher than those of H129-G4 at different time points, and the titer was approximately 10 times higher than that of H129-G4 at 48 h p.i. Similar results were obtained for low MOI (0.001) infection, and the titer of H129-Syn-G2 was double that of H129-G4 at 96 h p.i. Statistical analyses showed that H129-Syn-G2 had significantly more optimized growth properties than the parental virus, H129-G4 at MOI levels of 3 ($P < 0.0001$) and 0.001 ($P < 0.001$).

3.3. *The synthetic virus showed similar morphogenesis to that of the parental virus*

To compare the morphogenesis of H129-G4 and H129-Syn-G2 at different infection stages, infected cells were observed through transmission electron microscopy. At 12 h p.i., capsids (empty or filled) were observed in the nucleus of both samples, and the egress of capsids was observed in the margins of the nucleus (Fig. 5A and B). At 18 h p.i., in addition to the capsids, enveloped virions were observed in the cytoplasm of both samples (Fig. 5C and D). These results suggested that the morphogenesis of the synthetic virus was similar to that of the parental virus.

4. Discussion

HSV-1 H129 shows a unique anterograde spreading phenotype, making it a powerful tool for neuronal circuit tracing after proper modifications (Li et al., 2017; Yu et al., 2017; Su et al., 2020; Yang et al., 2020, 2022). In the present study, we designed and synthesized a complete HSV-1 genome based on H129-G4, a neuronal circuit tracer derived from H129 (Zeng et al., 2017). The H129-Syn-G2 genome was synthesized using a three-step recombination strategy, and the rescued virus showed similar cytopathic effects and morphogenesis to its parental virus H129-G4. Interestingly, growth curves at both high and

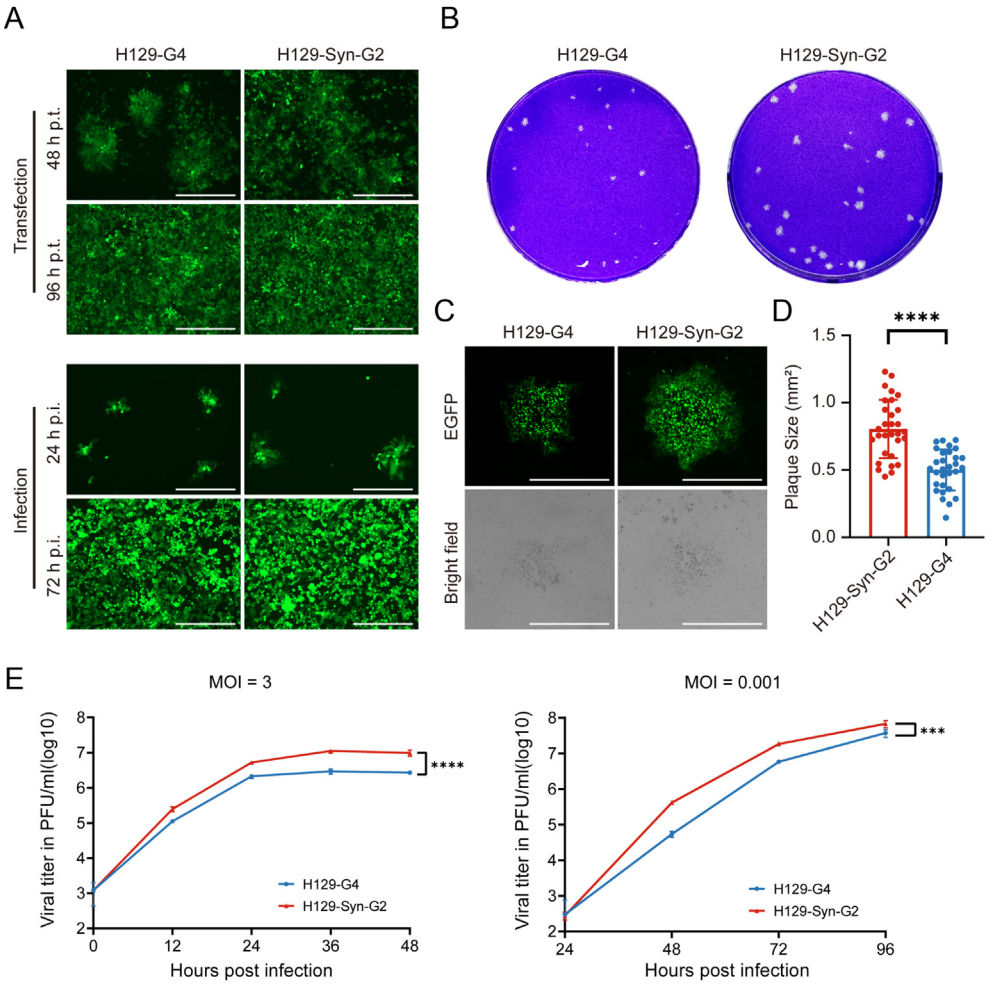

Fig. 4. Growth properties of H129-Syn-G2 and its parental virus. **A** Transfection and infection assay. Vero cells were transfected with BAC DNA of H129-G4 or H129-Syn-G2, and fluorescence was observed at 48 h and 96 h p.t. (upper panel). The supernatants harvested at 96 h p.t. were used to infect Vero cells, and fluorescence was observed at 24 h and 72 h p.i. (lower panel). Scale bars, 400 μm. **B** Plaque assay. Infected Vero cell monolayers were strained by crystalline violet and plaque was observed. **C** Microscopy of a representative plaque showing fluorescence and cytopathic effect. Vero cells were infected with H129-G4 or H129-Syn-G2 viruses. Images of fluorescence forming units were obtained under the Invitrogen EVOS FL Auto imaging system (upper panel) and typical cytopathic effects were observed at respective bright fields (lower panel). Scale bars, 1000 μm. **D** Statistical analysis of plaque size. Thirty plaques of each virus were randomly selected and the plaque size was measured. Statistical significance was determined using Student *t*-test (****$P < 0.0001$). **E** Growth curve analysis. Vero cells were infected individually with H129-G4 and H129-Syn-G2 at MOI levels of 3 and 0.001. Supernatants of infected cells were harvested at the indicated time point and titers were measured by plaque assay. Titers at each time point were represented by mean value ± standard deviation of three independent biological repeats. Statistical significance was determined using the ordinary two-way ANOVA test (***$P < 0.001$, ****$P < 0.0001$).

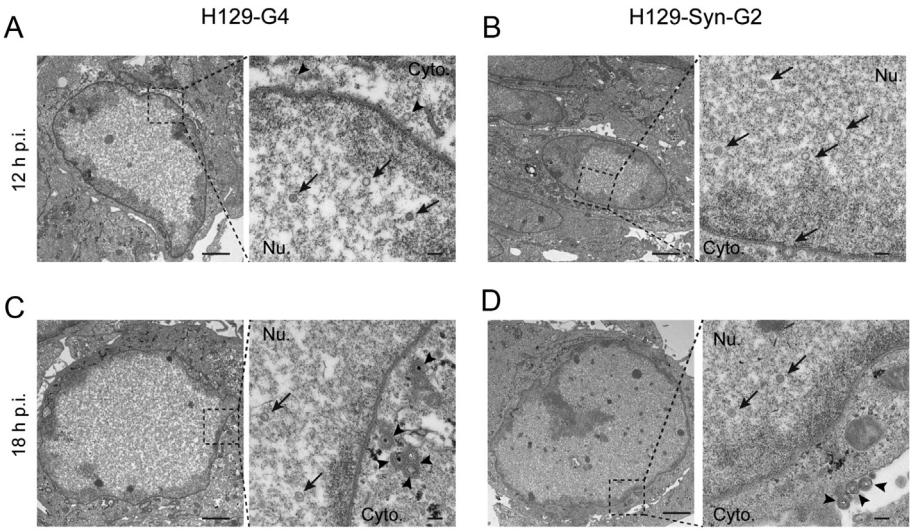

Fig. 5. Electron microscopy of H129-Syn-G2 and H129-G4. Vero cells were infected individually with H129-G4 or H129-Syn-G2 at an MOI of 1 and infected cells were harvested for transmission electron microscopy at 12 h post-infection (p.i.) (**A, B**) and 18 h p.i. (**C, D**). The boxes in the left panels were enlarged in the right panels. The viral capsids were indicated with arrows and enveloped virions were indicated as arrowheads. Cyto, cytoplasm; Nu, nucleus. Scale bars, 2 μm and 100 nm.

low MOIs showed that the infectious progeny production of the synthetic virus was significantly more optimized than that of the parental virus, H129-G4. The plaque size of the synthetic virus also appeared larger than that of H129-G4. This might be due to mutations or modifications in the synthetic virus. According to the results of Illumina sequencing, three mutations were made during the synthesis, which consequently impacted the viral proteins, UL23, UL24, and US11 (Table 1). The HSV-1 *UL23* gene encodes thymidine kinase (TK), which plays an important role in viral DNA synthesis (Munch-Petersen, 2010). Previous research revealed that there were six highly conserved region in UL23 (Sauerbrei et al., 2016), and the mutation we induced here (R20H) was not located in the conserved regions. The viral protein UL24 is important for replication and virulence (Dridi et al., 2018); however, it is unknown whether the A3V mutation affects the function of UL24. The viral protein US11 facilitates host shutdown (Charron et al., 2019), and previous research has suggested that 91–121 aa is essential for the RNA-binding function of US11 (Garzotti and Hamdan, 1998). The I72V mutation in the US11 of H129-Syn-G2 was not detected in this region. Overall, mutations in H129-Syn-G2 might contribute to the different properties of H129-G4 and H129-Syn-G2, but this needs to be further investigated in the future. Furthermore, a copy of the mGFP-2A-eGFP cassette and Cm^R were removed, and the BAC cassette was replaced with the pGF cassette, resulting in a slightly reduced genome size of H129-Syn-G2 (163,585 bp) compared to H129-G4 (164,424 bp). These changes may account for the different properties of the synthesized virus.

Previously, HSV-1 KOS^{YA} was synthesized using a TAR-based strategy with the HSV-1 KOS strain as the template (Oldfield et al., 2017). Interestingly, when the BAC cassette remained in the synthetic genome, the rescued virus showed reduced growth kinetics compared to the wild-type KOS, and only when the BAC cassette was removed from the genome did the rescued KOS^{YA} ex show replication properties similar to those of the wild-type KOS (Grzesik et al., 2018). In the present study, H129-Syn-G2 showed more optimized replication properties than H129-G4, although it retained the pGF vector cassette within the genome. Therefore, the impact of the vector sequence in the genome may be different and needs to be investigated on a case-by-case basis.

Compared with traditional genome modification methods, the synthetic platform could enhance the efficiency of multi-loci modifications of HSV-1 genome, which provides a powerful tool for engineering HSV-1 for different purposes. For neural circuit tracing, the most significant parameters of viral tracers include the labeling signal strength and cytotoxicity. Currently, labeling signals can be enhanced by carrying more fluorescent protein cassettes into the genome; however, high cytotoxicity hinders further development of the H129-based tracer (Xu et al., 2020; Yang et al., 2020). In the future, we plan to modify different foci in the H129-Syn-G2 genome to generate neuronal tracer viruses with attenuated toxicity. With the help of the synthetic platform, various attenuation strategies could be constructed and tested simultaneously, which may greatly improve the engineering efficiency. For oncolytic virus development, manipulation of multiple loci in the HSV-1 genome is needed for the deletion of virulence-associated genes, insertion of tumor-specific target genes, and immune checkpoint genes (Kaufman et al., 2015; Tian et al., 2022; Todo et al., 2022). With the help of a synthetic platform, virulence-associated genes can be modified to synthesize a series of attenuated recombinant viruses, and antitumor-associated foreign genes can be inserted. Furthermore, the development of the H129 synthetic platform can facilitate the evaluation of antiviral drugs and development of HSV-1 vaccines.

5. Conclusions

In summary, a synthetic H129-Syn-G2 virus was generated based on the parental virus H129-G4. The synthetic virus exhibited more optimized growth than the parental virus, and normal morphogenesis. This synthetic platform provides a useful tool for further manipulation of HSV-1 genomes for applications such as the attenuation of virulence, vaccine development, and oncolytic HSV modification.

Data availability

The genome sequence of H129-Syn-G2 has been submitted to GenBank under accession no OQ077661.

Ethics statement

This article does not contain any studies with human or animal subjects performed by any of the authors.

Author contributions

Han Xiao: conceptualization, investigation, methodology, software, visualization, writing-original draft. Hengrui Hu: investigation, methodology. Yijia Guo: investigation, methodology. Jiang Li: project administration. Le Wen: investigation. Wen-Bo Zeng: conceptualization, supervision, writing-reviewing and editing. Manli Wang:

conceptualization, supervision, writing-reviewing and editing. Min-Hua Luo: conceptualization, supervision, writing-reviewing and editing. Zhihong Hu: conceptualization, funding acquisition, supervision, writing-reviewing and editing.

Conflict of interest

The authors declare that there is no conflict of interest of the study. Min-Hua Luo is an editorial board member for *Virologica Sinica* and was not involved in the editorial review or the decision to publish this article.

Acknowledgments

The authors would like to thank Wuhan Institute of Virology for financial support for the research (grant no. EISA020201). We also acknowledge the core facility and technical support of Wuhan Institute of Virology for the technical support in transmission electron microscopy.

Appendix A. Supplementary data

Supplementary data to this article can be found online at https://doi.org/10.1016/j.virs.2023.03.005.

References

Abd-Aziz, N., Poh, C.L., 2021. Development of oncolytic viruses for cancer therapy. Transl. Res. 237, 98–123.
Aldrak, N., Alsaab, S., Algethami, A., Bhere, D., Wakimoto, H., Shah, K., Alomary, M.N., Zaidan, N., 2021. Oncolytic herpes simplex virus-based therapies for cancer. Cells 10, 1541.
Bradshaw, M.J., Venkatesan, A., 2016. Herpes simplex virus-1 encephalitis in adults: pathophysiology, diagnosis, and management. Neurotherapeutics 13, 493–508.
Charron, A.J., Ward, S.L., North, B.J., Ceron, S., Leib, D.A., 2019. The us11 gene of herpes simplex virus 1 promotes neuroinvasion and periocular replication following corneal infection. J. Virol. 93, e02246, 02218.
Chou, J., Kern, E.R., Whitley, R.J., Roizman, B., 1990. Mapping of herpes-simplex virus-1 neurovirulence to gamma-134.5, a gene nonessential for growth in culture. Science 250, 1262–1266.
Dix, R.D., McKendall, R.R., Baringer, J.R., 1983. Comparative neurovirulence of herpes simplex virus type 1 strains after peripheral or intracerebral inoculation of balb/c mice. Infect. Immun. 40, 103–112.
Dogrammatzis, C., Waisner, H., Kalamvoki, M., 2020. Non-essential" proteins of hsv-1 with essential roles in vivo: a comprehensive review. Viruses 13, 17.
Dridi, S., Richerioux, N., Gonzalez Suarez, C.E., Vanharen, M., Sanabria-Solano, C., Pearson, A., 2018. A mutation in the *ul24* gene abolishes expression of the newly identified ul24.5 protein of herpes simplex virus 1 and leads to an increase in pathogenicity in mice. J. Virol. 92, e00671-18.
Garzotti, M., Hamdan, M., 1998. Liquid chromatography tandem mass spectrometry of synthesis products associated with the viral protein u(s)11. Rapid Commun. Mass Spectrom. 12, 843–848.
Goldin, A.L., Sandri-Goldin, R.M., Levine, M., Glorioso, J.C., 1981. Cloning of herpes simplex virus type 1 sequences representing the whole genome. J. Virol. 38, 50–58.
Grzesik, P., Ko, N., Oldfield, L.M., Vashee, S., Desai, P.J., 2018. Rapid and efficient in vitro excision of bac sequences from herpesvirus genomes using cre-mediated recombination. J. Virol Methods 261, 67–70.
Hou, Z., Zhou, Z., Wang, Z., Xiao, G., 2016. Assembly of long DNA sequences using a new synthetic escherichia coli-yeast shuttle vector. Virol. Sin. 31, 160–167.
Hu, H., Pan, K., Shang, Y., Guo, Y., Xiao, H., Deng, F., Wang, M., Hu, Z., 2021. Multiloci manipulation of baculovirus genome reveals the pivotal role of homologous regions in viral DNA replication, progeny production, and enhancing transcription. ACS Synth. Biol. 11, 144–153.
Kaufman, H.L., Kohlhapp, F.J., Zloza, A., 2015. Oncolytic viruses: a new class of immunotherapy drugs. Nat. Rev. Drug Discov. 14, 642–662.
Kouprina, N., Larionov, V., 2008. Selective isolation of genomic loci from complex genomes by transformation-associated recombination cloning in the yeast saccharomyces cerevisiae. Nat. Protoc. 3, 371–377.
Kuny, C.V., Szpara, M.L., 2022. Alphaherpesvirus genomics: past, present and future. Curr. Issues Mol. Biol. 41–80.
Li, Y.D., Xu, J.M., Liu, Y.F., Zhu, J., Liu, N., Zeng, W.B., Huang, N., Rasch, M.J., Jiang, H.F., Gu, X., Li, X., Luo, M.H., Li, C.Y., Teng, J.L., Chen, J.G., Zeng, S.Q., Lin, L.N., Zhang, X.H., 2017. A distinct entorhinal cortex to hippocampal ca1 direct circuit for olfactory associative learning. Nat. Neurosci. 20, 559–570.
Ludlow, M., Kortekaas, J., Herden, C., Hoffmann, B., Tappe, D., Trebst, C., Griffin, D.E., Brindle, H.E., Solomon, T., Brown, A.S., Van Riel, D., Wolthers, K.C., Pajkrt, D., Wohlsein, P., Martina, B.E.E., Baumgärtner, W., Verjans, G.M., Osterhaus, A.D.M.E., 2016. Neurotropic virus infections as the cause of immediate and delayed neuropathology. Acta Neuropathol. 131, 159–184.
Macdonald, S.J., Mostafa, H.H., Morrison, L.A., Davido, D.J., 2012a. Genome sequence of herpes simplex virus 1 strain kos. J. Virol. 86, 6371–6372.
Macdonald, S.J., Mostafa, H.H., Morrison, L.A., Davido, D.J., 2012b. Genome sequence of herpes simplex virus 1 strain mckrae. J. Virol. 86, 9540–9541.
McGeoch, D.J., Dalrymple, M.A., Davison, A.J., Dolan, A., Frame, M.C., McNab, D., Perry, L.J., Scott, J.E., Taylor, P., 1988. The complete DNA-sequence of the long unique region in the genome of herpes-simplex virus type-1. J. Gen. Virol. 69, 1531–1574.
Messerle, M., Crnkovic, I., Hammerschmidt, W., Ziegler, H., Koszinowski, U.H., 1997. Cloning and mutagenesis of a herpesvirus genome as an infectious bacterial artificial chromosome. Proc. Natl. Acad. Sci. USA 94, 14759–14763.
Mineta, T., Rabkin, S.D., Yazaki, T., Hunter, W.D., Martuza, R.L., 1995. Attenuated multi-mutated herpes-simplex virus-1 for the treatment of malignant gliomas. Nat. Med. 1, 938–943.
Munch-Petersen, B., 2010. Enzymatic regulation of cytosolic thymidine kinase 1 and mitochondrial thymidine kinase 2: a mini review. Nucleos Nucleot. Nucleic Acids 29, 363–369.
Nassi, J.J., Cepko, C.L., Born, R.T., Beier, K.T., 2015. Neuroanatomy goes viral. Front. Neuroanat. 9, 80.
Oldfield, L.M., Grzesik, P., Voorhies, A.A., Alperovich, N., MacMath, D., Najera, C.D., Chandra, D.S., Prasad, S., Noskov, V.N., Montague, M.G., Friedman, R.M., Desai, P.J., Vashee, S., 2017. Genome-wide engineering of an infectious clone of herpes simplex virus type 1 using synthetic genomics assembly methods. Proc. Natl. Acad. Sci. USA 114, E8885–E8894.
Perng, Ghiasi H., Kaiwar, R., Nesburn, A.B., Wechsler, S.L., 1994. An improved method for cloning portions of the repeat regions of herpes-simplex virus type-1. J. Virol Methods 46, 111–116.
Perng, Mott, K.R., Osorio, N., Yukht, A., Salina, S., Nguyen, Q.-H., Nesburn, A.B., Wechsler, S.L., 2002. Herpes simplex virus type 1 mutants containing the kos strain icp34.5 gene in place of the mckrae icp34.5 gene have mckrae-like spontaneous reactivation but non-mckrae-like virulence. J. Gen. Virol. 83, 2933–2942.
Roizman, B., 1996. The function of herpes simplex virus genes: a primer for genetic engineering of novel vectors. Proc. Natl. Acad. Sci. USA 93, 11307–11312.
Sauerbrei, A., Bohn-Wippert, K., Kaspar, M., Krumbholz, A., Karrasch, M., Zell, R., 2016. Database on natural polymorphisms and resistance-related non-synonymous mutations in thymidine kinase and DNA polymerase genes of herpes simplex virus types 1 and 2. J. Antimicrob. Chemother. 71, 6–16.
Shang, Y., Wang, M., Xiao, G., Wang, X., Hou, D., Pan, K., Liu, S., Li, J., Wang, J., Arif, B.M., Vlak, J.M., Chen, X., Wang, H., Deng, F., Hu, Z., 2017. Construction and rescue of a functional synthetic baculovirus. ACS Synth. Biol. 6, 1393–1402.
Su, P., Ying, M., Han, Z., Xia, J., Jin, S., Li, Y., Wang, H., Xu, F., 2020. High-brightness anterograde transneuronal hsv1 h129 tracer modified using a trojan horse-like strategy. Mol. Brain 13, 5.
Su, P., Wang, H., Xia, J., Zhong, X., Hu, L., Li, Y., Li, Y., Ying, M., Xu, F., 2019. Evaluation of retrograde labeling profiles of hsv1 h129 anterograde tracer. J. Chem. Neuroanat. 100, 101662.
Sun, N., Cassell, M.D., Perlman, S., 1996. Anterograde, transneuronal transport of herpes simplex virus type 1 strain h129 in the murine visual system. J. Virol. 70, 5405–5413.
Szpara, Gatherer D., Ochoa, A., Greenbaum, B., Dolan, A., Bowden, R.J., Enquist, L.W., Legendre, M., Davison, A.J., 2014. Evolution and diversity in human herpes simplex virus genomes. J. Virol. 88, 1209–1227.
Szpara, M., Parsons, L., Enquist, L.W., 2010. Sequence variability in clinical and laboratory isolates of herpes simplex virus 1 reveals new mutations. J. Virol. 84, 5303–5313.
Tian, Y., Xie, D., Yang, L., 2022. Engineering strategies to enhance oncolytic viruses in cancer immunotherapy. Signal Transduct. Targeted Ther. 7, 117.
Todo, T., Ito, H., Ino, Y., Ohtsu, H., Ota, Y., Shibahara, J., Tanaka, M., 2022. Intratumoral oncolytic herpes virus g47Δ for residual or recurrent glioblastoma: a phase 2 trial. Nat. Med. 28, 1630–1639.
Vashee, S., Stockwell, T.B., Alperovich, N., Denisova, E.A., Gibson, D.G., Cady, K.C., Miller, K., Kannan, K., Malouli, D., Crawford, L.B., Voorhies, A.A., Bruening, E., Caposio, P., Fruh, K., 2017. Cloning, assembly, and modification of the primary human cytomegalovirus isolate toledo by yeast-based transformation-associated recombination. mSphere 2, 17.
Whitley, R.J., Roizman, B., 2001. Herpes simplex virus infections. Lancet 357, 1513–1518.
Xu, X.M., Holmes, T.C., Luo, M.H., Beier, K.T., Horwitz, G.D., Zhao, F., Zeng, W.B., Hui, M., Semler, B.L., Sandri-Goldin, R.M., 2020. Viral vectors for neural circuit mapping and recent advances in trans-synaptic anterograde tracers. Neuron 107, 1029–1047.
Yang, H., Xiong, F., Song, Y.-G., Jiang, H.-F., Qin, H.-B., Zhou, J., Lu, S., Grieco, S.F., Xu, X., Zeng, W.-B., Zhao, F., Luo, M.-H., 2020. Hsv-1 h129-derived anterograde neural circuit tracers: improvements, production, and applications. Neurosci. Bull. 37, 701–719.
Yang, H., Xiong, F., Qin, H.-B., Yu, Q.-T., Sun, J.-Y., Zhao, H.-W., Li, D., Zhou, Y., Zhang, F.-K., Zhu, X.-W., Wu, T., Jiang, M., Xu, X., Lu, Y., Shen, H.-J., Zeng, W.-B., Zhao, F., Luo, M.-H., 2022. A novel h129-based anterograde monosynaptic tracer exhibits features of strong labeling intensity, high tracing efficiency, and reduced retrograde labeling. Mol. Neurodegener. 17, 6.
Yu, K., Ahrens, S., Zhang, X., Schiff, H., Ramakrishnan, C., Fenno, L., Deisseroth, K., Zhao, F., Luo, M.-H., Gong, L., He, M., Zhou, P., Paninski, L., Li, B., 2017. The central amygdala controls learning in the lateral amygdala. Nat. Neurosci. 20, 1680–1685.
Zeng, W.-B., Jiang, H.-F., Gang, Y.-D., Song, Y.-G., Shen, Z.-Z., Yang, H., Dong, X., Tian, Y.-L., Ni, R.-J., Liu, Y., Tang, N., Li, X., Jiang, X., Gao, D., Androulakis, M., He, X.-B., Xia, H.-M., Ming, Y.-Z., Lu, Y., Zhou, J.-N., Zhang, C., Xia, X.-S., Shu, Y., Zeng, S.-Q., Xu, F., Zhao, F., Luo, M.-H., 2017. Anterograde monosynaptic transneuronal tracers derived from herpes simplex virus 1 strain h129. Mol. Neurodegener. 12, 38.